



Published in final edited form as:

Biomaterials. 2014 December ; 35(37): 9951–9962. doi:10.1016/j.biomaterials.2014.08.037.

Cerium oxide nanoparticles attenuate monocrotaline induced right ventricular hypertrophy following pulmonary arterial hypertension

Madhukar B. Kollia^{a,b,1}, Nandini D.P.K. Manne^{a,b,1}, Radhakrishna Para^b, Siva K. Nalabotu^{a,b}, Geeta Nandyala^b, Tolou Shokuhfar^c, Kun He^{c,d}, Azhang Hamlekhan^c, Jane Y. Ma^e, Paulette S. Wehner^f, Lucy Dornon^f, Ravikumar Arvapalli^b, Kevin M. Rice^b, and Eric R. Blough^{a,b,f,g,*}

^aDepartment of Pharmacology, Physiology and Toxicology, Marshall University, Joan C. Edwards School of Medicine, Huntington, WV, United States

^bCenter for Diagnostic Nanosystems, Marshall University, Huntington, WV, United States

^cDepartment of Mechanical Engineering and Engineering Mechanics, Michigan Technological University, Houghton, MI, United States

^dSchool of Materials Science and Engineering, Shandong University, Ji'nan, China

^eHealth Effects Laboratory Division, NIOSH, Morgantown, WV, United States

^fDepartment of Cardiology, Joan C. Edwards School of Medicine, Marshall University, Huntington, WV, United States

^gDepartment of Pharmaceutical Sciences and Research, Marshall University, Huntington, WV, United States

Abstract

Cerium oxide (CeO₂) nanoparticles have been posited to exhibit potent anti-oxidant activity which may allow for the use of these materials in biomedical applications. Herein, we investigate whether CeO₂ nanoparticle administration can diminish right ventricular (RV) hypertrophy following four weeks of monocrotaline (MCT)-induced pulmonary arterial hypertension (PAH). Male Sprague Dawley rats were randomly divided into three groups: control, MCT only (60 mg/kg), or MCT + CeO₂ nanoparticle treatment (60 mg/kg; 0.1 mg/kg). Compared to the control group, the RV weight to body weight ratio was 45% and 22% higher in the MCT and MCT + CeO₂ groups, respectively ($p < 0.05$). Doppler echocardiography demonstrated that CeO₂ nanoparticle treatment attenuated monocrotaline-induced changes in pulmonary flow and RV wall thickness. Paralleling these changes in cardiac function, CeO₂ nanoparticle treatment also

*Corresponding author. Center for Diagnostic Nanosystems, Room 241R, Robert C. Byrd Biotechnology Science Center Building, Department of Pharmaceutical Science and Research, 1700 3rd Ave., Marshall University, Huntington, WV 25755-1090, United States. Tel.: +1 304 696 2708; fax: +1 304 696 3766. blough@marshall.edu (E.R. Blough).

¹Authors contributed equally.

Disclaimer

The findings and conclusions in this report have not been formally disseminated by the NIOSH and should not be construed to represent any agency determination or policy.

Appendix A. Supplementary data

Supplementary data related to this article can <http://dx.doi.org/10.1016/j.biomaterials.2014.08.037>.

diminished MCT-induced increases in right ventricular (RV) cardiomyocyte cross sectional area, β -myosin heavy chain, fibronectin expression, protein nitrosylation, protein carbonylation and cardiac superoxide levels. These changes with treatment were accompanied by a decrease in the ratio of Bax/Bcl2, diminished caspase-3 activation and reduction in serum inflammatory markers. Taken together, these data suggest that CeO₂ nanoparticle administration may attenuate the hypertrophic response of the heart following PAH.

Keywords

Monocrotaline; Pulmonary arterial hypertension; Right ventricular hypertrophy; Cerium oxide nanoparticles

1. Introduction

Pulmonary arterial hypertension (PAH) is associated with the development of right ventricular (RV) hypertrophy which if allowed to proceed unchecked can lead to heart failure and death [1]. PAH is defined as an increase in mean pulmonary arterial pressure (PAPm) > 25 mm Hg at rest, or >30 mm Hg during exercise [2]. Although the pathogenesis of PAH is not fully understood, it is thought that disease progression is due, at least in part, to increases in nitric oxide, endothelin and prostanoids such as that seen frequently in patients with portal hypertension, congenital heart disease, and AIDS [3]. The treatment of PAH is largely symptomatic in nature and is centered around the administration of calcium channel blockers, diuretics, prostanoids, endothelin antagonists and lifestyle modifications. If improperly managed, the median life expectancy of patients with idiopathic PAH is approximately 2.8 years, with survival rates of 68%, 48%, and 34%, at 1-year, 3-year and 5-years, respectively [4]. Even with modern medical therapy, patients with PAH oftentimes experience disease progression and eventual referral for organ transplantation [5]. Despite advances in medical care the life expectancy of patients with PAH remains unacceptably low.

Cerium is the most abundant rare earth element that exhibits the ability to cycle between the Ce⁺³ (fully reduced) or Ce⁺⁴ (fully oxidized) state [6]. Recent data has suggested that CeO₂ nanoparticles can act as superoxide dismutase (SOD) and catalase mimetic [7,8], free radical scavenger [6,9] and that they can protect H₉C₂ cardiomyocytes from cigarette smoke extract-induced oxidative damage [10]. *In vivo* studies using the monocyte chemo-attractant protein-1 (MCP-1) transgenic mouse model of oxidative stress-induced cardiac hypertrophy have shown that CeO₂ nanoparticle administration can reduce the development of cardiac dysfunction and remodeling [11]. Similarly, other work has shown that CeO₂ nanoparticles attenuate carbon tetrachloride-induced oxidative stress [12], and that they can accelerate the decay of peroxynitrite [13]. Consistent with these findings, other data has suggested that the anti-oxidant activity of CeO₂ nanoparticles can protect liver against monocrotaline-induced hepatic toxicity [14]. Whether CeO₂ nanoparticle administration can attenuate the development of the RV hypertrophy seen during PAH is currently unclear.

Monocrotaline is a toxic pyrrolizidine alkaloid that is metabolized in the liver to monocrotaline pyrrole (MCTP) which can selectively injure lung endothelial cells causing

the infiltration of monocytes, and thickening of the pulmonary arterioles that precede the development of PAH [15,16]. The molecular mechanisms responsible for these MCT-induced changes are presently unclear; however recent reports have suggested that increases in oxidative stress and apoptosis, like that observed in the clinical development of PAH, are likely to play a role in the pathological remodeling of the heart [17]. The purpose of this study was to investigate whether the administration of CeO₂ nanoparticles can prevent the progression of RV hypertrophy following monocrotaline-induced PAH. We hypothesized that CeO₂ nanoparticles would attenuate MCT-induced increases in oxidative stress and systemic cytokine levels and that these reductions would be associated with diminished cardiac hypertrophy. Our data suggest that CeO₂ nanoparticle treatment may be effective in reducing the hypertrophic response seen following PAH in male Sprague Dawley rats.

2. Materials and methods

2.1. Animal model and experimental design

Animal care and surgical procedures were conducted in accordance with the guidelines provided by Marshall University Institutional Animal Care and Use Committee (IACUC), and Association for Assessment and Accreditation of Laboratory Animal Care (AAALAC). Seven week old (175–200 gm) male Sprague Dawley rats were purchased from Hilltop laboratories (Scottsdale, PA) and housed two per cage under a 12:12H dark–light cycle and maintained at 22 ± 2 °C. Rats were provided food and water *ad libitum* and allowed to acclimatize for at least 2 weeks before initiating the study. Periodic body weight and feed intake measurements were taken throughout the duration of the study. Rats were randomly assigned to one of three different groups: Control ($n = 6$), MCT only ($n = 6$), or MCT + CeO₂ nanoparticle treatment ($n = 6$). PAH was induced by a single injection of MCT (60 mg/kg S.C.) (Sigma–Aldrich, St. Louis, MO). Animals injected with MCT were given either CeO₂ nanoparticles (0.1 mg/kg *via* tail vein) (Nanoactive™ CeO₂ nanoparticles, NanoScale materials Inc., Manhattan, KS) or vehicle (deionized water) at the time of MCT administration and twice a week for 1st and 2nd week of the study. Animals were sacrificed after 28 days and the hearts and lungs were collected for further analysis.

2.2. Characterization of CeO₂ nanoparticles

The hydrodynamic particle size distribution was estimated using an LB-550 dynamic light scattering (DLS) particle size analyzer (Horiba scientific, Edison, NJ). Briefly, CeO₂ nanoparticles were sonicated in deionized water for 2 min to ensure equal dispersion. Particle size measurement was performed as outlined by the manufacturer in triplicate. Transmission electron microscopy was performed using JEOL JEM-2010 transmission electron microscope to determine the size of naked nanoparticles. Chemical characterization of the prepared CeO₂ nanoparticles was performed using a JEOL JSM-6320F Field Emission Scanning Electron Microscope (FESEM). Prior to analysis, nanoparticles were placed on a double-sided conductive carbon tape and attached to an aluminum stub. Noran Voyager EDX software was used to determine atomic and weight percentage of present elements according to their energy lines. X-ray photoelectron spectroscopy was performed to determine the relative amounts of Ce⁺³ and Ce⁺⁴ in the nanoparticles using a Kratos 165 XPS. A Scintag XDS 2000 powder diffractometer was used for the X-ray diffraction studies.

2.3. Echocardiography

Echocardiography was performed prior to the start of the study and at day 28 of the study as outlined previously [18]. Rats were anesthetized with an intraperitoneal injection of ketamine and xylazine cocktail mixture (50 mg/kg; 4:1) and the ventral thorax area shaved. ECG analysis was performed during the echocardiography procedure to monitor heart rate. Echocardiography measurements were obtained with a Philips Sonos 5500 echocardiogram system using 12-MHZ transducer. M-mode and 2-D modalities were used to measure RV and left ventricular (LV) wall thickness at the end of diastole using the right parasternal long axis view with the ultrasonic beam positioned perpendicular to the ventricular wall. Papillary muscles were used as reference point for measurements and to assure proper position in subsequent studies. Pulmonary artery flow was measured using pulsed wave Doppler at the pulmonary valve level while pulmonary artery diameter was measured at the level of pulmonary out flow tract during systole using the parasternal short axis view. An apical four-chamber view was employed to measure end-diastolic right ventricular area. Pulsed-wave Doppler was used to measure pulmonary artery acceleration time and flow.

2.4. Tissue processing and histological analysis

Animals were anesthetized with ketamine-xylazine (4:1) cocktail mixture (50 mg/kg, i.p) and supplemented as necessary to achieve loss of reflexive response. After a mid-ventral laparotomy, the heart was removed and placed in Krebs–Ringer bicarbonate buffer (KRB) containing 118 mM NaCl, 4.7 mM KCl, 2.5 mM CaCl₂, 1.2 mM KH₂PO₄, 1.2 mM MgSO₄, 24.2 mM NaHCO₃, and 10 mM D-glucose (pH 7.4) equilibrated with 5% CO₂/95% O₂ and maintained at 37°C. The right ventricle was separated from the left ventricle and septum, weighed and immediately flash frozen in liquid nitrogen before being stored at –80 °C for subsequent use.

RV tissues were sectioned (8 µm) using a Leica CM1950 cryostat and collected on poly-L-lysine coated slides. Sections were stained for dystrophin immunoreactivity and then evaluated for cardiomyocyte cross sectional area (CSA) as outlined elsewhere [19]. Briefly, sections were incubated for 30 min in a blocking solution (5% bovine serum albumin [BSA] in phosphate-buffered saline [PBS] containing 0.05% Tween 20 (PBS-T), pH 7.5) and then incubated with specific anti sera diluted in PBS-T (anti-dystrophin 1:100, rat-igG 1:100) for 1 h at 37°C. After washing with PBS-T, sections were incubated with FITC labeled secondary antibody (1:200) for 1 h at 37 °C. Muscle cross sections were visualized by epifluorescence using an Olympus BX51 microscope (Olympus, Center Valley, PA), fitted with 20× and 40× objectives.

Picrosirius red staining was used to assess the collagen content deposition in RV sections as detailed elsewhere [20]. Briefly, RV frozen tissue sections were fixed with 95% reagent alcohol for 1 min, washed three times with running tap water, and then stained with hematoxylin and picrosirius red. After dehydration and mounting, collagen content was visualized at 20× using an Olympus BX51 microscope (Olympus, Center Valley, PA).

The fluorescent superoxide marker dihydroethidium was used to evaluate superoxide levels as outlined elsewhere [21]. Briefly, RV frozen tissue sections were washed with phosphate-

buffered saline (PBS) for 5 min and then incubated with 200 μ l of 10 μ M of dihydroethidium (Molecular Probes, Eugene, OR) for 1 h at room temperature. After washing with PBS (3 \times 5 min), fluorescence was visualized under a Texas red filter using an Olympus BX-51 microscope (Olympus America, Melville, NY, USA) equipped with an Olympus WH 20 \times wide field objective. Images were recorded digitally using a CCD camera and the integrated optical density determined using the Alpha view image analysis software (Cell Biosciences, Inc., Santa Clara, CA).

2.5. SDS PAGE and immunoblotting

Frozen right ventricles were homogenized in T-PER buffer (2 mL/g tissue; Pierce, Rockford, IL, USA) containing protease and phosphatase inhibitors (P8340 and P5726, Sigma–Aldrich, St. Louis, MO, USA). Samples were incubated on ice for 30 min and the supernatant was collected by centrifugation at 12,000 \times g for 10 min at 4 $^{\circ}$ C. The concentration of protein in the supernatant was determined *via* the 660 nm assay (Piercenet, Rockford, IL). Samples were mixed with Laemmli sample buffer (Sigma–Aldrich, St. Louis, MO, USA) and heated for 5 min at 95 $^{\circ}$ C. Forty micrograms of total protein were separated on 10% PAGER Gold Precast gels (Lonza, Rockland, ME) and then transferred to nitrocellulose membranes using standard methods as detailed elsewhere [21,22]. Membranes were blocked with 5% milk in Tris Buffered Saline (TBS) containing 0.05% Tween-20 (TBST) for 1 h and then probed with primary antibodies for the detection of β -myosin heavy chain (Sigma Aldrich, St. Louis, MO), fibronectin (Abcam, Cambridge, MA), p-ERK1/2, ERK1/2, p-JNK, JNK, Bax, Bcl2, caspase-3, cleaved caspase-3, GAPDH (Cell Signaling Technology, Inc., Beverly, MA) and 3-nitrotyrosine (Santa Cruz Biotechnology, Inc., Santa Cruz, CA). After an overnight incubation at 4 $^{\circ}$ C in primary antibody buffer (5% BSA in TBST, primary antibody diluted 1:1000) membranes were washed with TBST, and then incubated with HRP-conjugated secondary antibodies (anti-rabbit or anti-mouse, Cell Signaling Technology, Danvers, MA) for 1 h at room temperature. Protein bands were visualized following reaction with ECL reagent (GE Healthcare Bio-Sciences Corp., Piscataway, NJ). Proteins of interest were quantified using AlphaEaseFC image analysis software (Alpha Innotech, San Leandro, CA) and normalized to glyceraldehyde 3-phosphate dehydrogenase (GAPDH).

2.6. OxyBlot analysis

An OxyBlotTM Protein Oxidation Detection kit (Millipore, MA) was used for quantification of carbonyl groups. Briefly, 5 μ g total protein of each sample was derivatized by reaction with 2, 4-dinitrophenylhydrazine (DNPH) at room temperature for 15 min before undergoing separation on 10% PAGER Gold Precast gels. Oxidized proteins were detected by immunoblotting using the anti-DNP antibody provided in the kit. Bands were visualized following reaction with ECL reagent (Amersham ECL Western Blotting reagent RPN 2106, GE Healthcare Bio-Sciences Corp., Piscataway, NJ). Target protein levels were quantified by AlphaView SA image analysis software (Alpha Innotech, San Leandro, CA).

2.7. Serum protein immune assays

Sera collected during exsanguation were pooled from all six rats in each group and sent to Myriad RBM (Austin, TX) for RodentMAP® v 2.0 Antigen analysis using a Luminex Lab MAP instrument. Each analyte was quantified using 4 and 5 parameter, weighted and non-weighted curve fitting algorithms using proprietary data analysis software developed at Rules-Based Medicine.

2.8. Data analysis

Results are presented as mean \pm standard error of mean. Data were analyzed using SigmaPlot 11.0 statistical software. One-way analysis of variance (ANOVA) was used for comparison among different groups followed by Student Newman Keuls *post hoc* test to determine statistical significance. A *p*-value of 0.05 was considered to be statistically significant.

3. Results

3.1. Characterization of CeO₂ nanoparticles

The hydrodynamic diameter of the CeO₂ nanoparticles as determined by DLS was 300 ± 58 nm while TEM analysis with a corresponding scattered area diffraction pattern indicated a particle diameter between 10 and 30 nm (Fig. 1 Panels A, B, and C). Energy dispersive X-ray spectroscopy (EDS) confirmed the presence of cerium and oxygen (Fig. 1 Panel D). X-ray photoelectron spectroscopy showed the presence of cerium in both the Ce⁺³ and Ce⁺⁴ states (Fig. 1 Panel E). X-ray diffraction (XRD) confirmed the cubic fluorite structure of the nanoparticles (Fig. 1, Panel F).

3.2. CeO₂ nanoparticle treatment decrease MCT-induced increases in right ventricular tissue hypertrophy

Compared to the control group, body weight in the MCT and MCT + CeO₂ nanoparticle treated groups was 14% and 13% less, respectively ($P < 0.05$). Conversely, the heart weight to body weight ratio was 22% higher and 4% higher in the MCT and MCT + CeO₂ groups when compared with that observed in the control group ($P < 0.05$). Similarly, the RV weight to body weight ratio was 83% and 29% higher in the MCT and MCT + CeO₂ nanoparticle groups ($P < 0.05$), while the lung weight to body weight ratio was 48% and 36% higher in the MCT and MCT + CeO₂ nanoparticle groups, respectively ($P < 0.05$, Table 1).

3.3. CeO₂ nanoparticle treatment decreases MCT-induced changes in pulmonary arterial pressure and cardiac remodeling

Compared to the MCT + CeO₂ nanoparticle treatment group, echocardiographic analysis of pulmonary arterial flow demonstrated a mid-systolic notch in the MCT group (Fig. 2, Panel B). Consistent with this finding, pulmonary arterial pressure (PA Pr), mean pulmonary arterial diameter (MPA diameter), mean pulmonary arterial area (MPA area) and right ventricular outflow tract diameter (RVOT) were 18%, 27%, 46%, and 14% higher in MCT group at day 28 when compared to that observed at the start of the study (Fig. 2, Panels E, F, G, and H, $P < 0.05$). There were no significant differences in pulmonary arterial pressure,

mean pulmonary arterial diameter, mean pulmonary arterial area and right ventricular outflow tract diameter between the measurements taken at day 1 and day 28 in the MCT + CeO₂ nanoparticle treatment group (Fig. 2, Panels E, F, G, and H). Similar to our findings at the whole tissue level, echocardiographic analysis demonstrated that CeO₂ nanoparticle treatment attenuated MCT-induced increases in RV anterior free wall thickness (Fig. 3, Panel E, $P < 0.05$). Likewise, the inter-ventricular septum diameter was 16% higher in MCT animals (Fig. 3, Panel F, $P < 0.05$) but only 3% greater in the MCT + CeO₂ animals between day 1 and day 28 of the study (Fig. 3, Panel F).

To examine the molecular alterations that might accompany PAH-induced changes in RV thickness we next performed immunofluorescence staining for dystrophin to determine the average cardiomyocyte cross sectional area (CSA) in the right ventricle. Compared to the control animals, ventricular CSA was 34% higher in the MCT animals but only 1% greater in the MCT + CeO₂ group (Fig. 4, Panels A, B, C, D, $P < 0.05$). Picrosirius red staining indicated that the degree of MCT-induced collagen deposition was less in the MCT + CeO₂ treated group when compared to that in the MCT group (Fig. 4, Panels G vs F).

In an effort to extend these findings, we next performed immunoblotting to examine the effect of CeO₂ nanoparticles treatment on fibronectin and myosin heavy chain expression. Compared to control group, MCT-induced fibronectin expression was 113% higher in the MCT group but only 4% more in the MCT + CeO₂ group (Fig. 5, Panel A, $P < 0.05$). Similarly, MHC- β expression was 91% higher in the MCT group but only 3% higher in MCT + CeO₂ group (Fig. 5, Panel B, $P < 0.05$).

3.4. CeO₂ nanoparticle treatment attenuates MCT-induced increases in cardiac oxidative stress

As an indicator for oxidative stress, we determined superoxide anion levels in tissue sections obtained from the RV by quantifying dihydroethidium (DHE) fluorescence levels. Compared to the control group, the DHE fluorescence intensity was 71% higher and 12% lower in the MCT and MCT + CeO₂ nanoparticle treatment group, respectively (Fig. 6, Panels A, B, C, and D; $P < 0.05$). In an effort to extend these findings, we next examined the effects of PAH and treatment on the amount of protein exhibiting 3-nitrotyrosine (3-NT) modification. Compared to the control group, 3-NT levels were 15% higher in the MCT group. Interestingly, CeO₂ nanoparticle treatment significantly reduced 3-NT levels by 17% compared to that observed in the control group (Fig. 7, Panel A, $P < 0.05$). Likewise, compared to control group, the amount of protein carbonylation was 14% higher significantly in the MCT group and 4% higher in MCT + CeO₂ group (Fig. 7, Panel B, $P < 0.05$).

The mitogen activated protein kinases (MAPK) have been shown to be activated by increased oxidative stress [23]. Compared to the control group, p-JNK levels were 19% and 11% higher in the MCT and MCT + CeO₂ groups, respectively (Fig. 8, Panel A, $P < 0.05$). Compared to the control animals, the amount of p-ERK 1/2 protein was 17% higher and 7% lower in MCT and MCT + CeO₂ animals, respectively (Fig. 8, Panel B, $P < 0.05$).

3.5. CeO₂ nanoparticle treatment decreases MCT-induced cardiomyocyte apoptosis

To extend upon above findings, we next examined the effects of CeO₂ nanoparticle treatment on Bax and Bcl-2 expression. Compared to control group, the ratio of Bax/Bcl-2 was 84% higher in the MCT but only 29% higher in the MCT + CeO₂ group (Fig. 9, Panel A, $P < 0.05$). Compared to control animals, total caspase-3 protein expression levels were 82% and 21% higher in the MCT and MCT + CeO₂ nanoparticle treatment groups, respectively. Similarly, the amount of cleaved caspase-3 (19 kDa) was 19% higher in the MCT animals but only 1% higher in the MCT + CeO₂ treatment group (Fig. 9, Panel B, $P < 0.05$).

3.6. CeO₂ nanoparticle treatment decreases serum inflammatory markers

Compared to control group, MCT insult appeared to increase the amount of serum C-reactive protein (CRP), TNF- α , CD40 Ligand, serum amyloid protein, von Willebrand factor, vascular endothelial growth factor A, macrophage inflammatory protein-1 beta, macrophage colony-stimulating factor-1, and tissue inhibitor of metalloproteinase-1 while treatment with CeO₂ nanoparticle appeared to attenuate these inflammatory markers (Supplementary Fig. 1).

4. Discussion

Despite significant advancement in our understanding of the physiological and molecular events that underlie the development of PAH, the morbidity and mortality associated with this disease remains unacceptably high. The use of nanomaterials for therapeutic applications is in its infancy and has thus far largely centered on the investigation of this technology for the treatment of cancer. Given the unique anti-oxidant and anti-inflammatory properties exhibited by CeO₂ nanoparticles, we sought to determine if they could be used to attenuate the development of PAH in a rat model that is thought to model many of the cellular and molecular events observed in the human condition [24,25].

It is hypothesized that monocrotaline induces the development of PAH by selectively damaging pulmonary endothelial cells which causes an increase in pulmonary vascular resistance [15,16,26]. Under normal conditions, pulmonary artery flow velocity increases and decreases slowly in a symmetric fashion. Conversely, with pulmonary arterial hypertension, flow velocity increases and decreases rapidly due alterations in vessel stiffness [27]. Consistent with previous work [28], monocrotaline insult was associated with right ventricular hypertrophy (Table 1), alterations in the pulmonary arterial flow (Fig. 2B), and increases in pulmonary arterial pressure (Fig. 2E), diameter (Fig. 2F), arterial area (Fig. 2G), and ventricular out flow tract diameter (Fig. 2H). Importantly, we found that PAH associated increases RV tissue weight, right ventricular anterior free wall thickness, and ventricular septal diameter were diminished with CeO₂ nanoparticle treatment (Table 1, Fig. 3).

In an effort to better characterize the hypertrophic response, we next investigated whether monocrotaline induced increases in right ventricular mass were associated with cardiomyocyte hypertrophy and fibrosis. Consistent with our echocardiographic findings, our histological studies demonstrated that CeO₂ nanoparticle treatment diminished

monocrotaline-induced increases in right ventricular cardiomyocyte cross sectional area (Fig. 4), cardiac fibrosis (Fig. 4, Panel E, F, G) and fibronectin levels (Fig. 5A).

Like that seen in skeletal muscle, the regulation of myosin in the heart is dynamic. It is thought that expression of the alpha myosin heavy chain (MHC) predominates in the normal heart [29] however, with cardiac hypertrophy there is a gradual upregulation of the β -MHC to reflect the altered contractile demands of the growing heart [30]. In the present study, and similar to previous work [31], we found that MCT-induced increases in cardiac mass were associated with increases in β -MHC expression (Fig. 5B) and importantly, that this upregulation was attenuated following CeO₂ nanoparticle administration (Fig. 5B).

It has been postulated that increases in oxidative stress may be involved in the initiation and progression of cardiac hypertrophy [32]. Previous studies have shown that CeO₂ nanoparticles act as an effective free radical scavenger and that this unique ability can be exploited for the treatment of stroke and cardiomyopathy where elevations in oxidative stress may play a pathological role in disease progression [11,33]. Consistent with these previous studies and other work demonstrating the anti-oxidant activity of CeO₂ nanoparticles [34], we found that CeO₂ nanoparticles treatment was associated with decreased tissue superoxide anion levels (Fig. 6, Panels A, B, C, and D), diminished protein tyrosine nitration (Fig. 7, Panel A) and an attenuation in the amount of MCT-induced protein carbonylation (Fig. 7, Panel B). Whether the changes we observe are entirely due to the anti-oxidant activity of CeO₂ nanoparticles or are related to increases in anti-oxidant activity are currently not clear and will require additional experimentation.

Recent work has suggested that MAPK signaling is regulated, at least in part, by oxidative stress [35,36] and that antioxidants can function to block the activation of these molecules both *in vitro* and *in vivo* [37,38]. Other data has demonstrated that the MAPK signaling pathways are important regulators of ventricular remodeling following pressure overload [37]. Supporting these findings, we found that MCT-induced right ventricular hypertrophy was associated with increased phosphorylation (activation) of JNK-MAPK and ERK 1/2 and that this effect was diminished with CeO₂ nanoparticles treatment (Fig. 8 Panel A, B).

Previous data has suggested that cardiomyocyte apoptosis may be involved in the ventricular remodeling seen during MCT-induced PAH [39]. To explore this possibility, we next examined the ratio of Bax/Bcl2 ratio. It is thought that Bax is a pro-apoptotic member of Bcl-2 family and that this protein plays an important role in mediating cell death during both physiological and pathological conditions [40]. In contrast to the pro-apoptotic effects of Bax, Bcl-2 is an anti-apoptotic molecule that functions to inhibit Bax and prevent cellular apoptosis [41]. As such, a diminished Bax/Bcl-2 ratio is suggestive of cellular apoptosis while an increase in the ratio of Bax/Bcl-2 is anti-apoptotic [42]. Here, we found that CeO₂ nanoparticle treatment was associated with diminished MCT-induced increases in the Bax/Bcl2 ratio (Fig. 9, Panel A) along with caspase-3 cleavage which is a marker for apoptosis (Fig. 9, Panel B). It is thought that inflammation plays a significant role in MCT-induced PAH [43]. In humans, the involvement of leukocytes and macrophages in the inflammatory process leading to the development of PAH associated vascular lesions is well documented [44,45]. In the current study, we found that MCT administration was associated with the

upregulation of several serum protein markers associated with inflammation (e.g. C-reactive protein (CRP), tissue necrosis factor alpha (TNF- α)) and that this upregulation was attenuated with CeO₂ nanoparticle treatment (Supplementary Fig. 1).

5. Conclusion

In summary, our data demonstrates that CeO₂ nanoparticle treatment diminishes the development of monocrotaline-induced pulmonary arterial hypertension and right ventricular remodeling in the rat by decreasing oxidative stress and cardiomyocyte apoptosis. These data suggest that additional studies examining the potential efficacy of using CeO₂ nanoparticles for the treatment of PAH may be warranted. Given the expected stability of these particles over time in the absence of refrigeration or other special handling may make therapies incorporating the use of CeO₂ nanoparticles attractive for the treatment of disease in developing countries and other austere environments. Future studies involving a combinatorial approach to PAH therapy which includes CeO₂ nanoparticles and other currently available treatment modalities such as use of diuretics, calcium channel blockers or prostacyclin analogues is a potential area of future interest.

Supplementary Material

Refer to Web version on PubMed Central for supplementary material.

Acknowledgments

This work was supported in part from DOE grant (DE-PS02-09 ER-01 to E.R.B).

References

1. Sztrymf B, Souza R, Bertoletti L, Jais X, Sitbon O, Price LC, et al. Prognostic factors of acute heart failure in patients with pulmonary arterial hypertension. *Eur Respir J*. 2010; 35:1286–93. [PubMed: 19897557]
2. Humbert M, Sitbon O, Chaouat A, Bertocchi M, Habib G, Gressin V, et al. Pulmonary arterial hypertension in France: results from a national registry. *Am J Respir Crit Care Med*. 2006; 173:1023–30. [PubMed: 16456139]
3. McLaughlin VV, McGoon MD. Pulmonary arterial hypertension. *Circulation*. 2006; 114:1417–31. [PubMed: 17000921]
4. Galie N, Manes A, Branzi A. Evaluation of pulmonary arterial hypertension. *Curr Opin Cardiol*. 2004; 19:575–81. [PubMed: 15502501]
5. Houtchens J, Martin D, Klinger JR. Diagnosis and management of pulmonary arterial hypertension. *Pulm Med*. 2011; 2011:845864. [PubMed: 21941650]
6. Rzigalinski BA. Nanoparticles and cell longevity. *Technol Cancer Res Treat*. 2005; 4:651–9. [PubMed: 16292885]
7. Heckert EG, Karakoti AS, Seal S, Self WT. The role of cerium redox state in the SOD mimetic activity of nanoceria. *Biomaterials*. 2008; 29:2705–9. [PubMed: 18395249]
8. Pirmohamed T, Dowding JM, Singh S, Wasserman B, Heckert E, Karakoti AS, et al. Nanoceria exhibit redox state-dependent catalase mimetic activity. *Chem Commun*. 2010; 46:2736–8.
9. Hirst SM, Karakoti AS, Tyler RD, Sriranganathan N, Seal S, Reilly CM. Anti-inflammatory properties of cerium oxide nanoparticles. *Small*. 2009; 5:2848–56. [PubMed: 19802857]
10. Niu J, Wang K, Kolattukudy PE. Cerium oxide nanoparticles inhibit oxidative stress and nuclear factor-kappaB activation in H9c2 cardiomyocytes exposed to cigarette smoke extract. *J Pharmacol Exp Ther*. 2011; 338:53–61. [PubMed: 21464334]

11. Niu J, Azfer A, Rogers LM, Wang X, Kolattukudy PE. Cardioprotective effects of cerium oxide nanoparticles in a transgenic murine model of cardiomyopathy. *Cardiovasc Res.* 2007; 73:549–59. [PubMed: 17207782]
12. Hirst SM, Karakoti A, Singh S, Self W, Tyler R, Seal S, et al. Bio-distribution and in vivo antioxidant effects of cerium oxide nanoparticles in mice. *Environ Toxicol.* 2013; 28:107–18. [PubMed: 21618676]
13. Dowding JM, Seal S, Self WT. Cerium oxide nanoparticles accelerate the decay of peroxynitrite (ONOO). *Drug Deliv Transl Res.* 2013; 3:375–9. [PubMed: 23936755]
14. Amin KA, Hassan MS, Awad el ST, Hashem KS. The protective effects of cerium oxide nanoparticles against hepatic oxidative damage induced by monocrotaline. *Int J Nanomedicine.* 2011; 6:143–9. [PubMed: 21289991]
15. Roth RA, Reindel JF. Lung vascular injury from monocrotaline pyrrole, a putative hepatic metabolite. *Adv Exp Med Biol.* 1991; 283:477–87. [PubMed: 1906225]
16. Wilson DW, Segall HJ, Pan LC, Dunston SK. Progressive inflammatory and structural changes in the pulmonary vasculature of monocrotaline-treated rats. *Microvasc Res.* 1989; 38:57–80. [PubMed: 2503687]
17. Redout EM, van der Toorn A, Zuidwijk MJ, van de Kolk CW, van Echteld CJ, Musters RJ, et al. Antioxidant treatment attenuates pulmonary arterial hypertension-induced heart failure. *Am J Physiol Heart Circ Physiol.* 2010; 298:H1038–47. [PubMed: 20061549]
18. Walker Jr EM, Morrison RG, Dornon L, Laurino JP, Walker SM, Studeny M, et al. Acetaminophen combinations protect against iron-induced cardiac damage in gerbils. *Ann Clin Lab Sci.* 2009; 39:378–85. [PubMed: 19880766]
19. Wang Y, Wu M, Al-Rousan R, Liu H, Fannin J, Paturi S, et al. Iron-induced cardiac damage: role of apoptosis and deferasirox intervention. *J Pharmacol Exp Ther.* 2011; 336:56–63. [PubMed: 20947636]
20. Dolber PC, Spach MS. Picrosirius red staining of cardiac muscle following phosphomolybdic acid treatment. *Stain Technol.* 1987; 62:23–6. [PubMed: 2438817]
21. Wang C, Blough ER, Arvapalli R, Dai X, Paturi S, Manne N, et al. Metabolic syndrome-induced tubulointerstitial injury: role of oxidative stress and preventive effects of acetaminophen. *Free Radic Biology Med.* 2013; 65:1417–26.
22. Katta A, Kundla S, Kakarla SK, Wu M, Fannin J, Paturi S, et al. Impaired overload-induced hypertrophy is associated with diminished mTOR signaling in insulin-resistant skeletal muscle of the obese Zucker rat. *Am J Physiol Regul Integr Comp Physiol.* 2010; 299:R1666–75. [PubMed: 20926758]
23. Kumar D, Lou H, Singal PK. Oxidative stress and apoptosis in heart dysfunction. *Herz.* 2002; 27:662–8. [PubMed: 12439637]
24. Cai X, Seal S, McGinnis JF. Sustained inhibition of neovascularization in vldlr^{-/-} mice following intravitreal injection of cerium oxide nanoparticles and the role of the ASK1-P38/JNK-NF-kappaB pathway. *Biomaterials.* 2014; 35:249–58. [PubMed: 24140045]
25. Das S, Dowding JM, Klump KE, McGinnis JF, Self W, Seal S. Cerium oxide nanoparticles: applications and prospects in nanomedicine. *Nanomedicine.* 2013; 8:1483–508. [PubMed: 23987111]
26. Chen L, Gan XT, Haist JV, Feng Q, Lu X, Chakrabarti S, et al. Attenuation of compensatory right ventricular hypertrophy and heart failure following monocrotaline-induced pulmonary vascular injury by the Na⁺-H⁺ exchange inhibitor cariporide. *J Pharmacol Exp Ther.* 2001; 298:469–76. [PubMed: 11454907]
27. Koskenvuo JW, Mirsky R, Zhang Y, Angeli FS, Jahn S, Alastalo TP, et al. A comparison of echocardiography to invasive measurement in the evaluation of pulmonary arterial hypertension in a rat model. *Int J Cardiovasc Imaging.* 2010; 26:509–18. [PubMed: 20140524]
28. Hessel MH, Steendijk P, den Adel B, Schutte CI, van der Laarse A. Characterization of right ventricular function after monocrotaline-induced pulmonary hypertension in the intact rat. *Am J Physiol Heart Circ Physiol.* 2006; 291:H2424–30. [PubMed: 16731643]

29. Locher MR, Razumova MV, Stelzer JE, Norman HS, Patel JR, Moss RL. Determination of rate constants for turnover of myosin isoforms in rat myocardium: implications for in vivo contractile kinetics. *Am J Physiol Heart Circ Physiol*. 2009; 297:H247–56. [PubMed: 19395549]
30. Herron TJ, McDonald KS. Small amounts of alpha-myosin heavy chain isoform expression significantly increase power output of rat cardiac myocyte fragments. *Circ Res*. 2002; 90:1150–2. [PubMed: 12065316]
31. Kogler H, Hartmann O, Leineweber K, Nguyen van P, Schott P, Brodde OE, et al. Mechanical load-dependent regulation of gene expression in monocrotaline-induced right ventricular hypertrophy in the rat. *Circ Res*. 2003; 93:230–7. [PubMed: 12842921]
32. Madamanchi NR, Runge MS. Redox signaling in cardiovascular health and disease. *Free Radic Biology Med*. 2013; 61C:473–501.
33. Estevez AY, Pritchard S, Harper K, Aston JW, Lynch A, Lucky JJ, et al. Neuroprotective mechanisms of cerium oxide nanoparticles in a mouse hippo-campal brain slice model of ischemia. *Free Radic Biology Med*. 2011; 51:1155–63.
34. Chen J, Patil S, Seal S, McGinnis JF. Rare earth nanoparticles prevent retinal degeneration induced by intracellular peroxides. *Nat Nanotechnol*. 2006; 1:142–50. [PubMed: 18654167]
35. Son Y, Cheong YK, Kim NH, Chung HT, Kang DG, Pae HO. Mitogen-activated protein kinases species: how can ROS activate MAPK pathways? *J Signal Transduct*. 2011; 2011:792639. [PubMed: 21637379]
36. Arad M, Seidman CE, Seidman JG. AMP-activated protein kinase in the heart: role during health and disease. *Circ Res*. 2007; 100:474–88. [PubMed: 17332438]
37. McCubrey JA, Lahair MM, Franklin RA. Reactive oxygen species-induced activation of the MAP kinase signaling pathways. *Antioxid Redox Signal*. 2006; 8:1775–89. [PubMed: 16987031]
38. Dyck JR, Lopaschuk GD. AMPK alterations in cardiac physiology and pathology: enemy or ally? *J Physiol*. 2006; 574:95–112. [PubMed: 16690706]
39. Yang DL, Zhang HG, Xu YL, Gao YH, Yang XJ, Hao XQ, et al. Resveratrol inhibits right ventricular hypertrophy induced by monocrotaline in rats. *Clin Exp Pharmacol Physiol*. 2010; 37:150–5. [PubMed: 19566840]
40. Wolter KG, Hsu YT, Smith CL, Nechushtan A, Xi XG, Youle RJ. Movement of Bax from the cytosol to mitochondria during apoptosis. *J Cell Biol*. 1997; 139:1281–92. [PubMed: 9382873]
41. Gross A, McDonnell JM, Korsmeyer SJ. BCL-2 family members and the mitochondria in apoptosis. *Genes Dev*. 1999; 13:1899–911. [PubMed: 10444588]
42. Porichi O, Nikolaidou ME, Apostolaki A, Tserkezoglou A, Arnogiannaki N, Kassanos D, et al. BCL-2, BAX and P53 expression profiles in endometrial carcinoma as studied by real-time PCR and immunohistochemistry. *Anticancer Res*. 2009; 29:3977–82. [PubMed: 19846939]
43. Hassoun PM, Mouthon L, Barbera JA, Eddahibi S, Flores SC, Grimminger F, et al. Inflammation, growth factors, and pulmonary vascular remodeling. *J Am Coll Cardiol*. 2009; 54:S10–9. [PubMed: 19555853]
44. Price LC, Wort SJ, Perros F, Dorfmueller P, Huertas A, Montani D, et al. Inflammation in pulmonary arterial hypertension. *Chest*. 2012; 141:210–21. [PubMed: 22215829]
45. Carr MW, Roth SJ, Luther E, Rose SS, Springer TA. Monocyte chemoattractant protein 1 acts as a T-lymphocyte chemoattractant. *Proc Natl Acad Sci U S A*. 1994; 91:3652–6. [PubMed: 8170963]

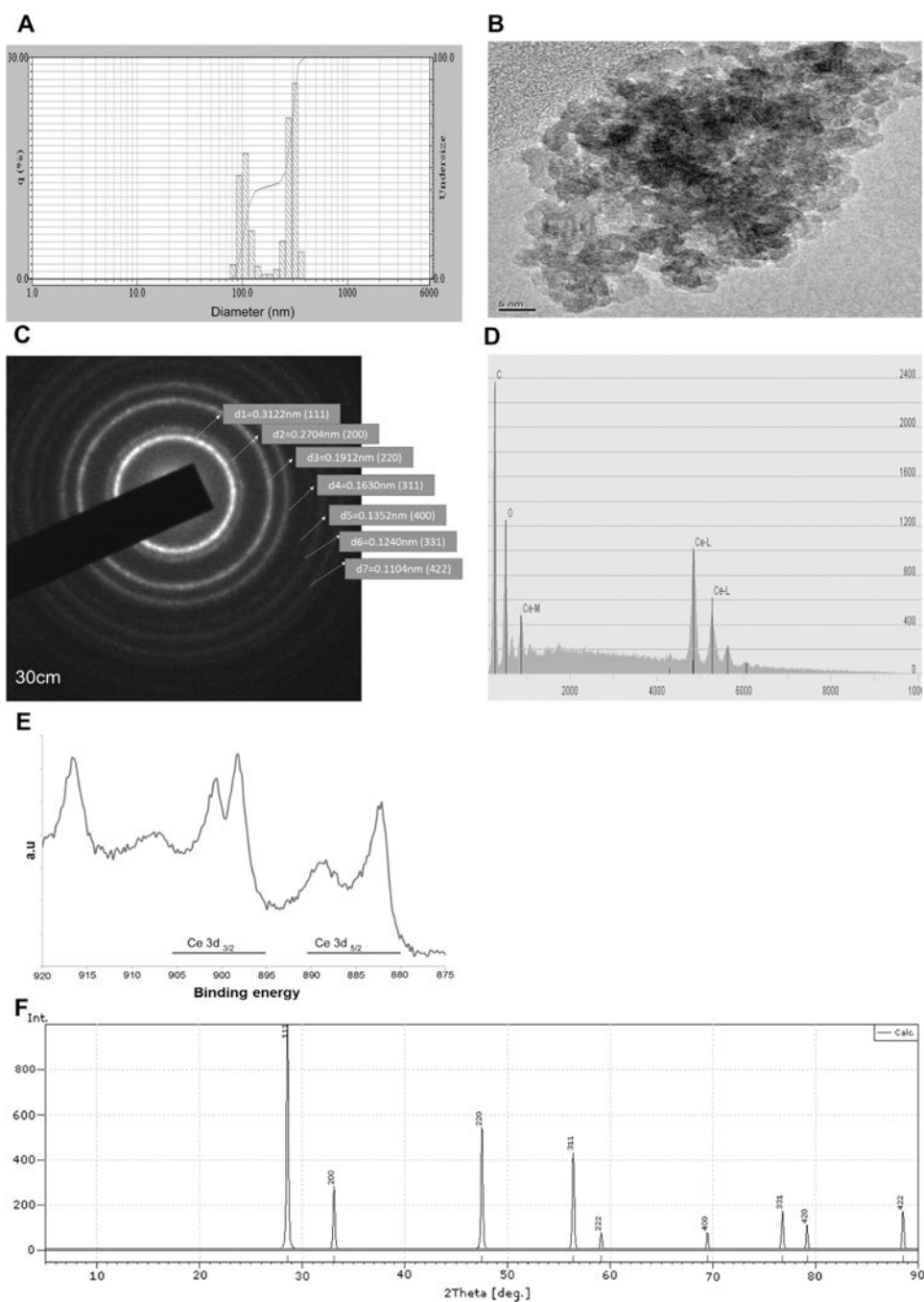


Fig. 1. Characterization of CeO₂ nanoparticles

Nanoparticle size was determined by dynamic light scattering (DLS) (Panel A) and transmission electron microscopy (TEM) (Panel B). Corresponding scattered area diffraction is shown (Panel C). Energy dispersive X-ray spectroscopy shows the presence of cerium and oxygen in the nanoparticles (Panel D). X-ray photoelectron spectroscopy shows the relative amounts of Ce⁺³ and Ce⁺⁴ in the nanoparticles (Panel E). X-ray diffraction of the nanoparticles demonstrates the typical lattice structure (Panel F).

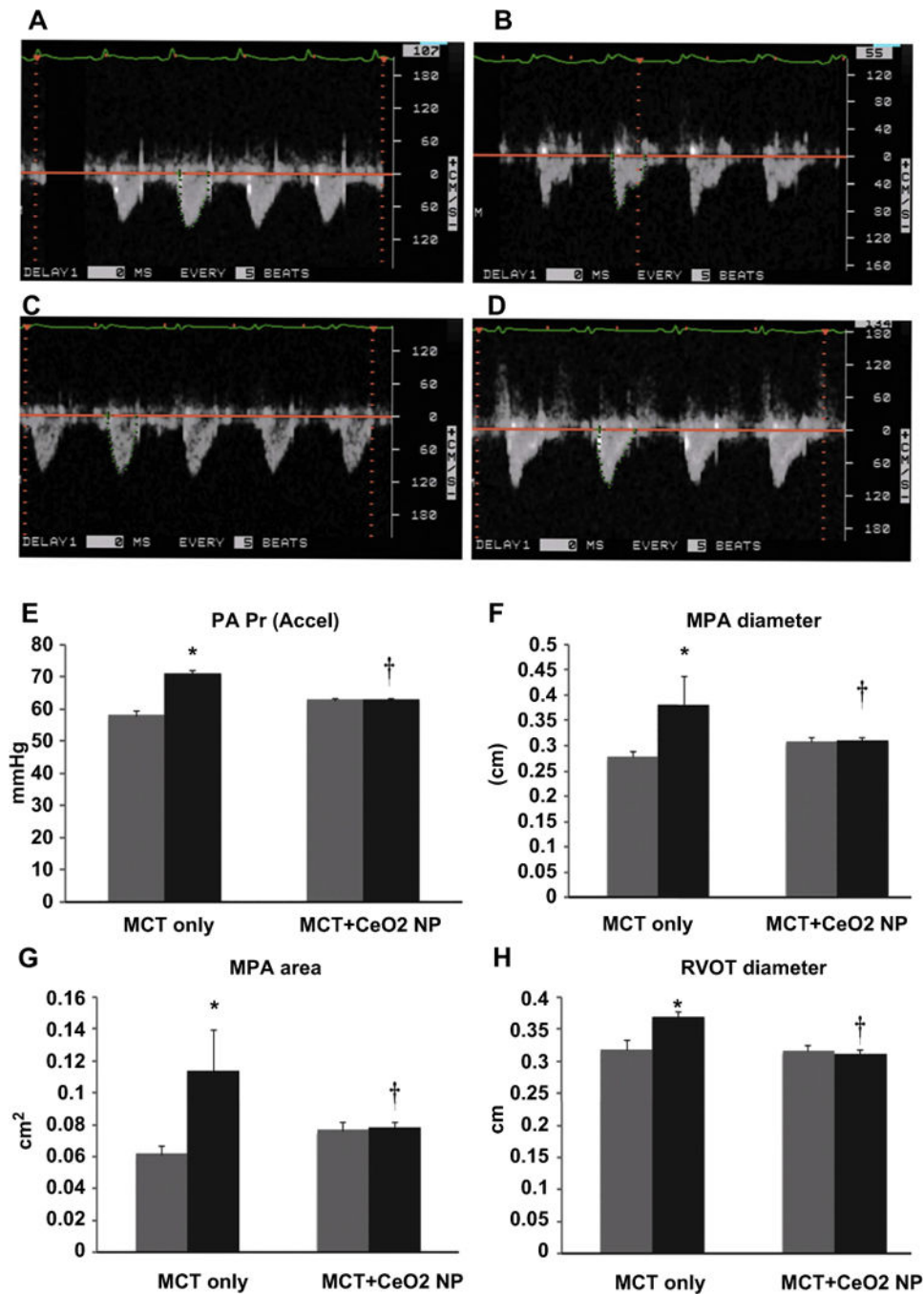


Fig. 2. CeO₂ nanoparticle treatment improves pulmonary flow and diminishes pulmonary artery remodeling

Pulsed-wave Doppler echocardiography demonstrating normal, round shaped flow profile at baseline (day 1) in the MCT rats (Panel A) and triangular flow profile with mid-systolic notching on day 28 (Panel B). Normal, round shaped flow profile at baseline (day 1) in the MCT + CeO₂ nanoparticle treated rats (Panel C) and the continuation of the normal, round shaped flow profile observed with CeO₂ nanoparticle treatment at day 28 of treatment (Panel D). Pulsed-wave Doppler echocardiography quantified data for pulmonary arterial pressure (Panel E), mean pulmonary arterial diameter (Panel F), mean pulmonary arterial area (Panel

G), right ventricular outflow tract diameter (Panel H). Data are mean \pm SEM ($n = 6$ rats/group). Grey columns indicate readings at day 1 while black columns denote readings at day 28. *Significantly different from base line values of MCT only group. † Significantly different from day 28 values of MCT only group ($P < 0.05$). (For interpretation of the references to colour in this figure legend, the reader is referred to the web version of this article.)

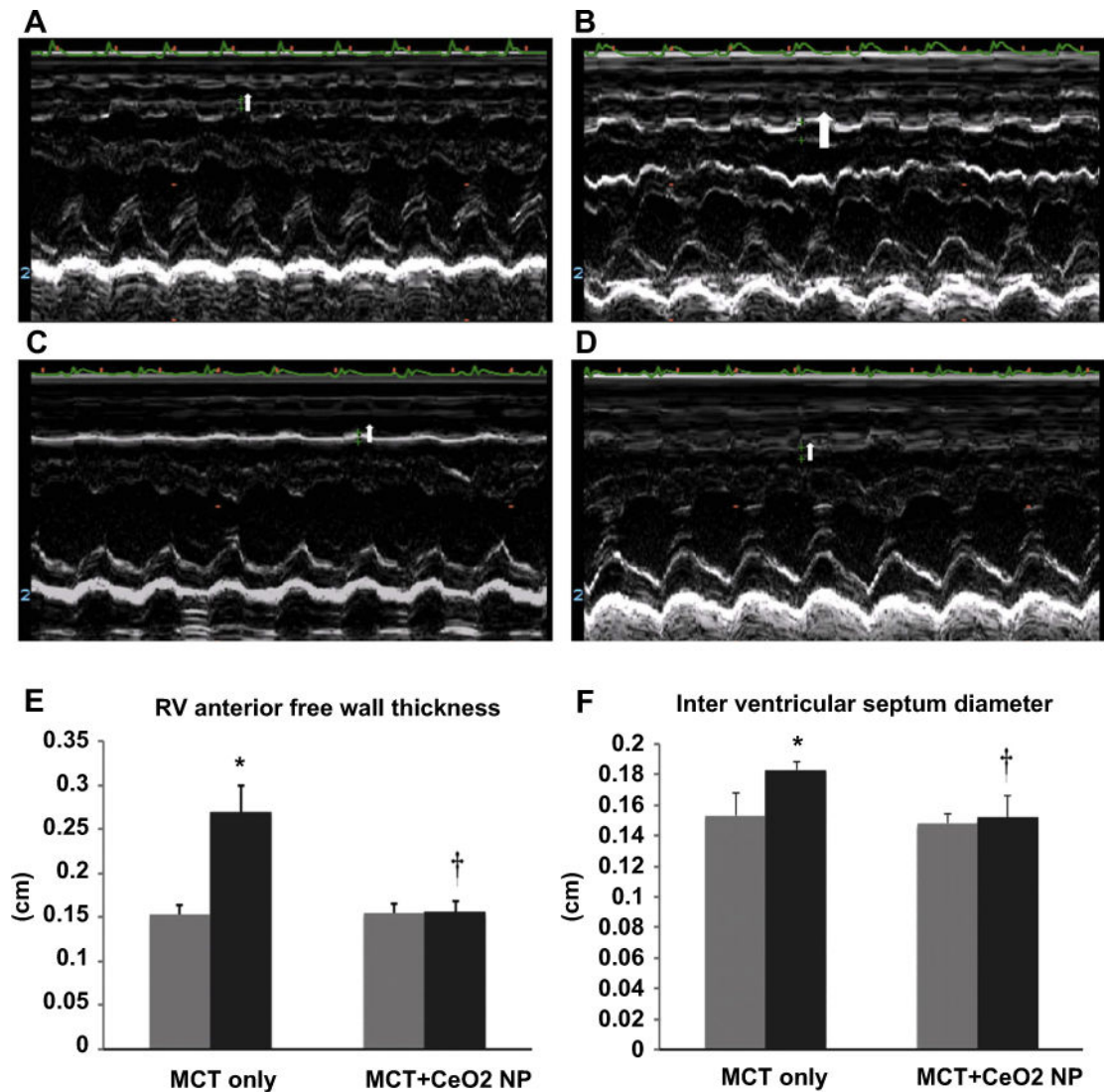


Fig. 3. CeO₂ nanoparticle treatment attenuates MCT-induced increases in right ventricle wall thickness and cardiac remodeling

M-mode echocardiography images representing right ventricle wall thickness of the MCT only rats on day 1 (Panel A) and at day 28 (Panel B) or the MCT + CeO₂ nanoparticle treated group on day 1 (Panel C) and at day 28 (Panel D). Ventricle wall thickness (Panel E) and intra-ventricular septum diameter (Panel F) in the MCT only and MCT treated groups. Data are mean \pm SEM, ($n = 6$ rats/group). Grey columns indicate readings at day 1 while black columns denote readings at day 28. *Significantly different from base line values of MCT only group. † Significantly different from day 28 values of MCT only group ($P < 0.05$). (For interpretation of the references to colour in this figure legend, the reader is referred to the web version of this article.)

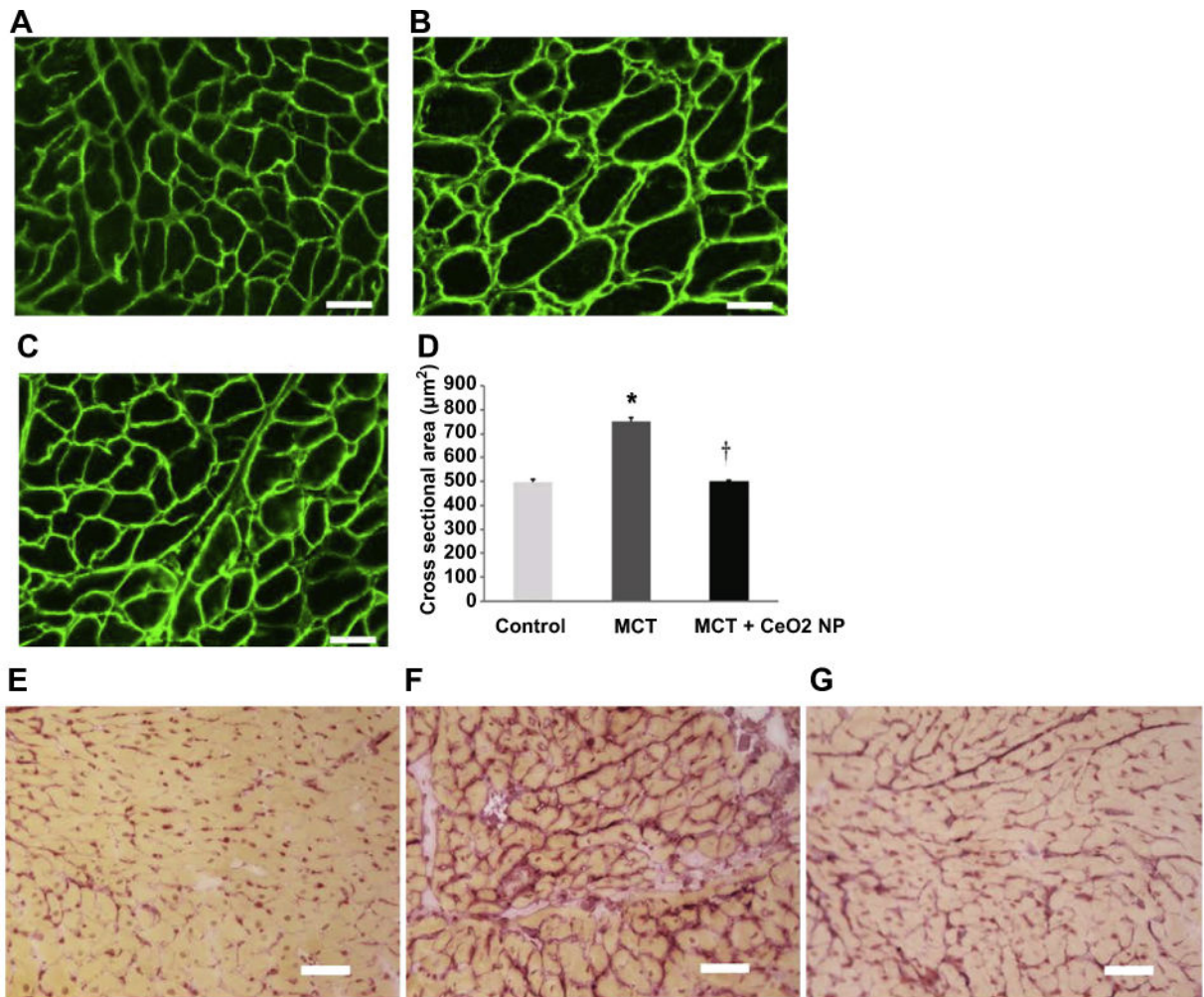


Fig. 4. CeO₂ nanoparticle administration attenuates monocrotaline-induced increases in cardiomyocyte cross sectional area and cardiac fibrosis

Dystrophin stained right ventricular sections from control (Panel A), MCT only (Panel B), and MCT + CeO₂ nanoparticle treatment group (Panel C). Quantification of cardiomyocyte cross sectional area (Panel D). Picosirius red staining was used to evaluate cardiac fibrosis in the right ventricles of control (Panel E), MCT only (Panel F) and MCT + CeO₂ nanoparticle treatment groups (Panel G). Scale bar = 50 µm. Data are mean ± SEM ($n = 3$ rats/group). * Significantly different from control. † Significantly different from the MCT only group ($P < 0.05$).

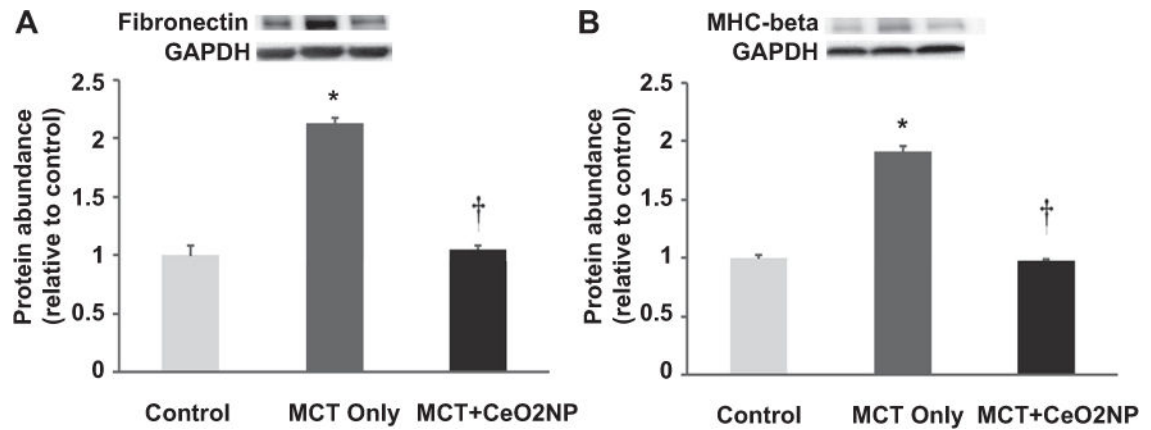


Fig. 5. MCT induced increases in RV fibronectin and MHC-beta are attenuated with cerium oxide nanoparticle treatment

Protein isolates from the right ventricle of control, MCT only, MCT + CeO₂ nanoparticle treated groups were analyzed by immunoblotting for changes in fibronectin (Panel A) and myosin heavy chain-beta (Panel B) protein levels. Protein abundance was normalized to the expression of GAPDH. *n* = 6 for each group. * Significantly different from control. † Significantly different from the MCT only group (*P* < 0.05).

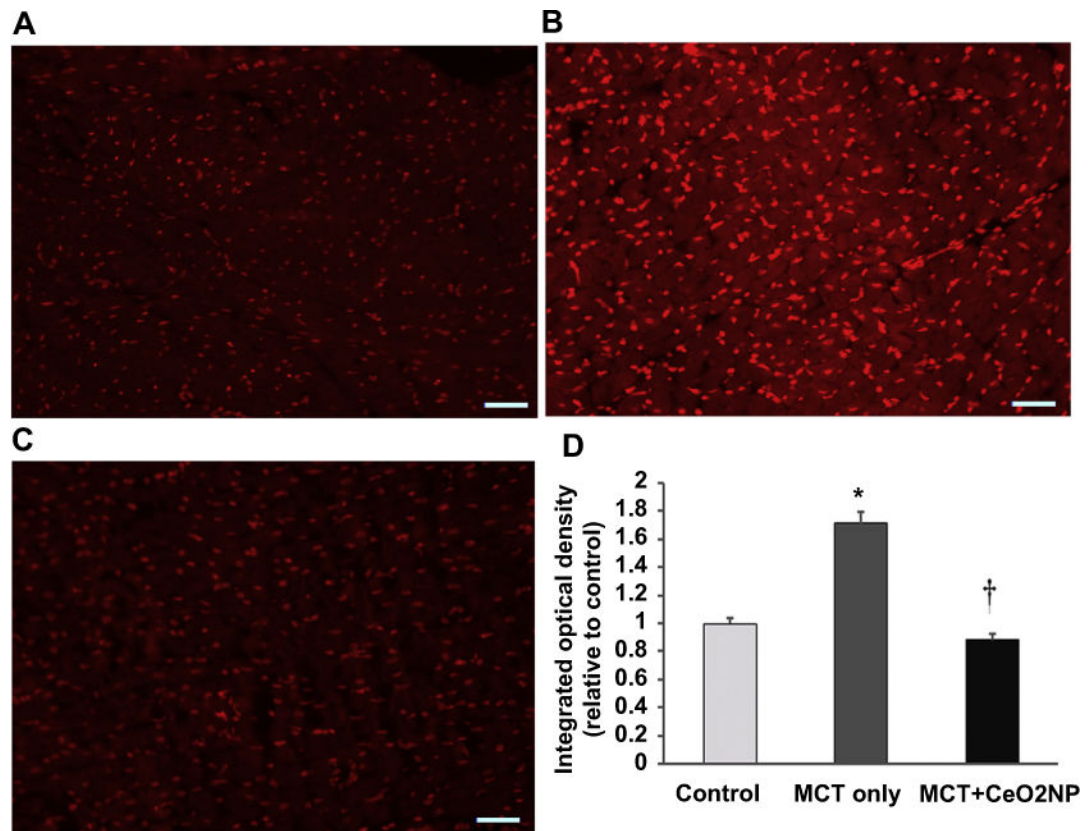


Fig. 6. Histological analysis of RV tissue sections demonstrates attenuation of monocrotaline induced increase in superoxide levels by cerium oxide nanoparticles

Dihydroethidium stained right ventricular sections from control (Panel A), MCT only (Panel B), and MCT + CeO₂ nanoparticle treatment group (Panel C) at 28 days. Quantification of intensity of dihydroethidium staining (Panel D). Scale bar 50 μ m $n = 3$ animals/group. * Significantly different from control. † Significantly different from the MCT only group ($P < 0.05$).

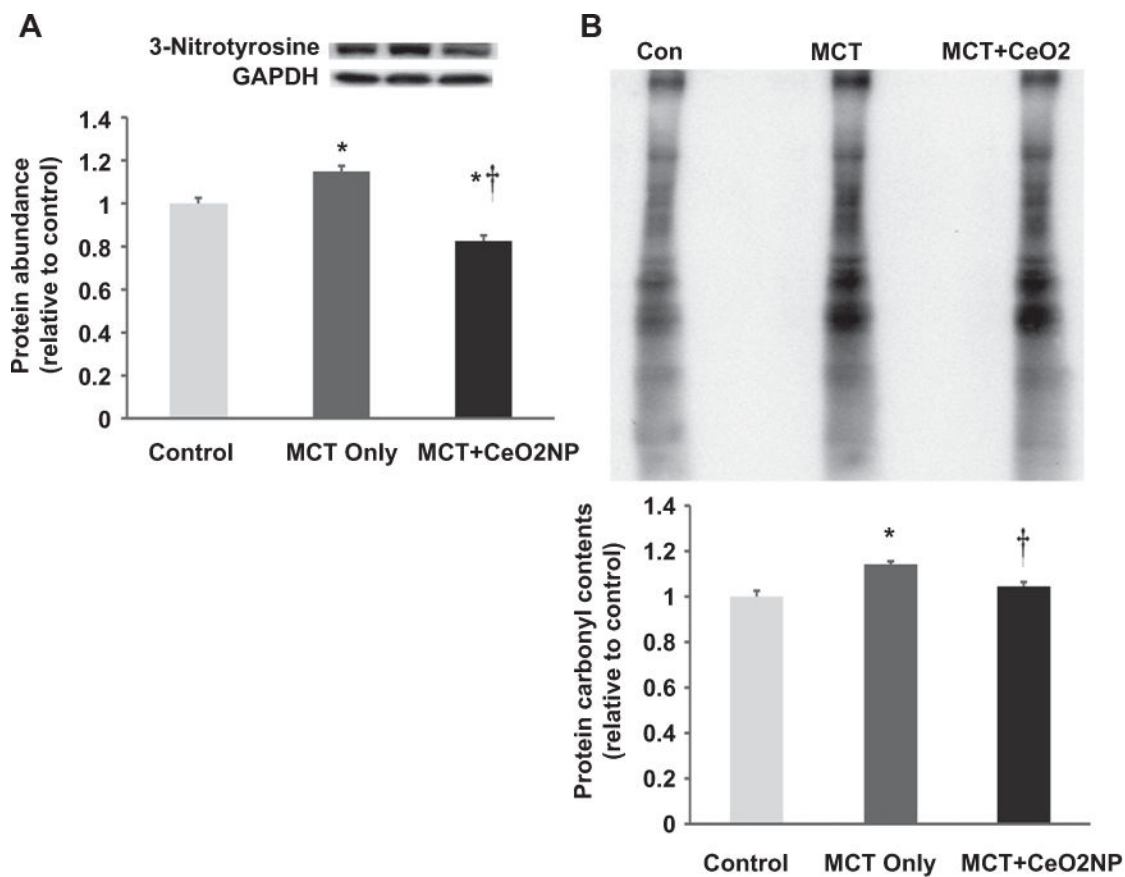


Fig. 7. Cerium oxide nanoparticle treatment decreases MCT-induced increases in protein nitration and carbonylation

Protein isolates obtained from the right ventricles of control, MCT only and MCT + CeO₂ nanoparticle treated groups were analyzed by immunoblotting for alterations in protein 3-nitrosylation (Panel A) and carbonylation (Panel B). * Significantly different from control. † Significantly different from the MCT only group ($P < 0.05$). $n = 6$ animals/group.

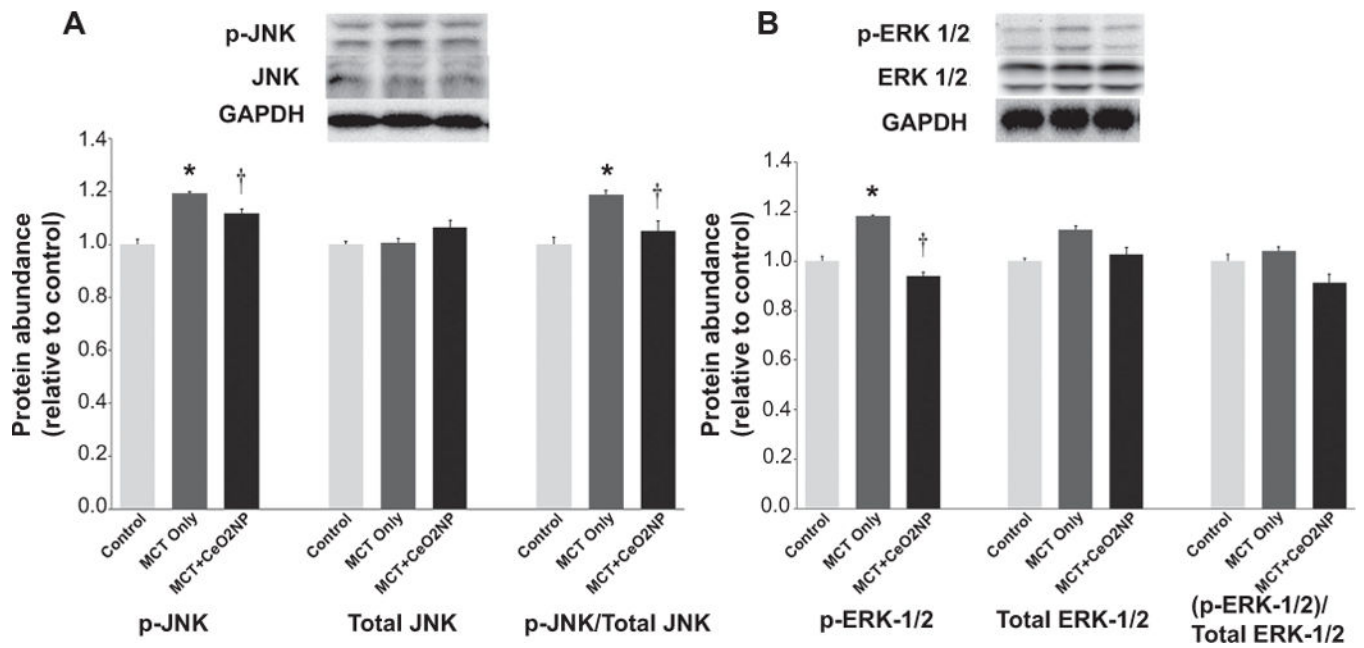


Fig. 8. Immunoblot analysis of RV tissue demonstrates attenuation of monocrotaline induced increase in markers of oxidative stress by cerium oxide nanoparticles

Protein isolates of RV from control, MCT only and MCT + CeO₂ nanoparticles treated group was analyzed by immunoblotting to determine the amount of p-JNK, total JNK (Panel A), p-ERK1/2, and total ERK1/2 (Panel B) normalized to the expression of GAPDH. * Significantly different from control. † Significantly different from the MCT only group ($P < 0.05$). $n = 6$ animals/group.

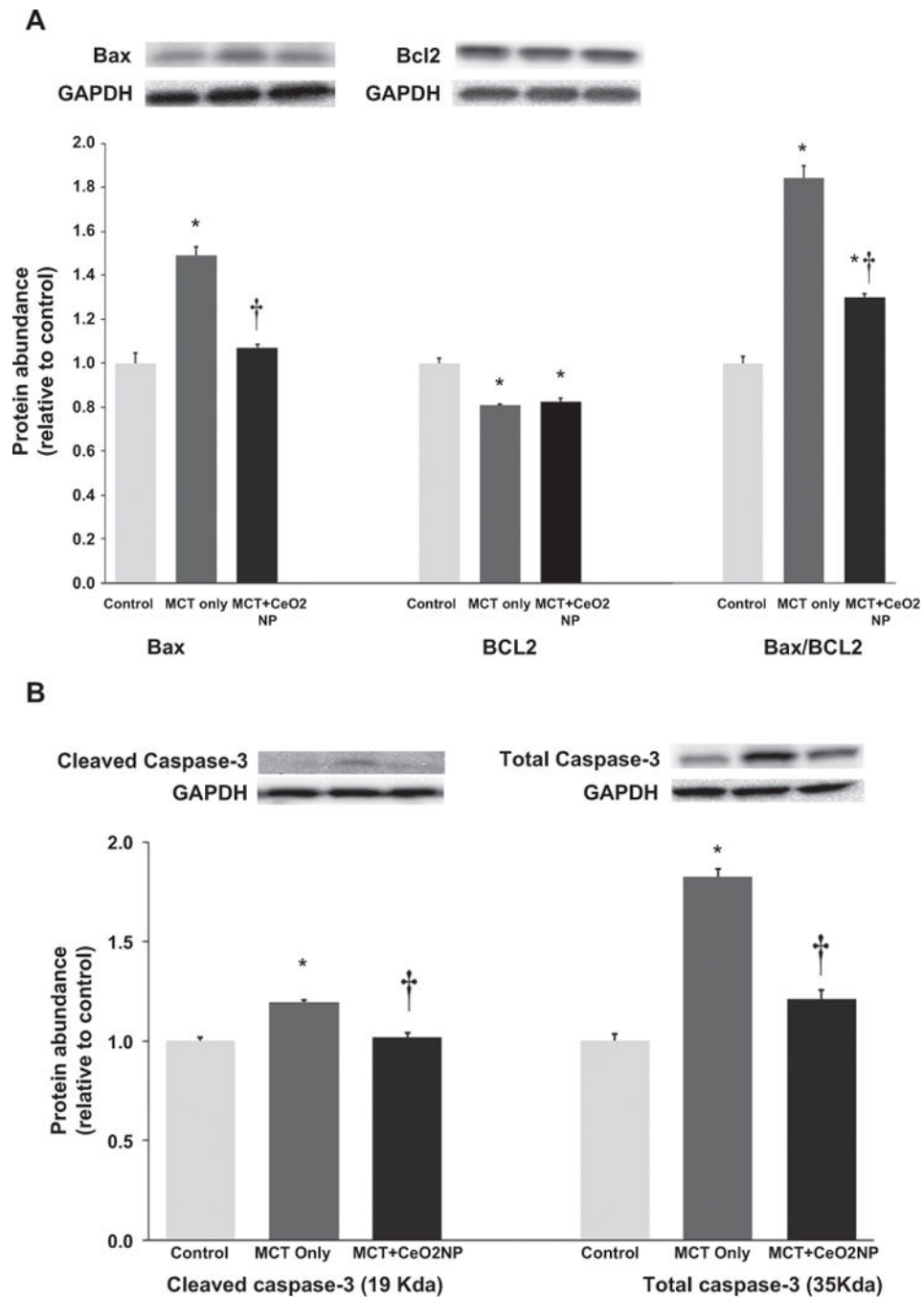


Fig. 9. Cerium oxide nanoparticle treatment attenuates MCT-induced increases in markers of apoptosis

Protein isolates of RV from control, MCT only and MCT + CeO₂ nanoparticles treated groups was analyzed by immunoblotting to determine the amount of Bax and Bcl2 and normalized to the expression of GAPDH (Panel A). Amount of cleaved caspase 3, and total caspase 3 normalized to the expression of GAPDH (Panel B). * Significantly different from control. † Significantly different from the MCT only group ($P < 0.05$). $n = 6$ animals/group.

Table 1

Cerium oxide nanoparticle treatment attenuates monocrotaline-induced increases in right ventricular remodeling.

Weight	Control group	MCT only group	MCT + CeO₂ group
Initial body weight (g)	265.0 ± 5.0	266.7 ± 2.79	255.7 ± 2.73
Final body weight (g)	408.3 ± 10.8	349.6 ± 9.46 ^a	356.3 ± 3.48 ^a
Change in body weight (g)	143.3 ± 6.42	99.2 ± 5.19 ^a	110.3 ± 5.79 ^a
Final heart weight (g)	1.178 ± 0.01	1.233 ± 0.13	1.080 ± 0.02
Heart weight to body weight ratio	2.89 ± 0.07	3.53 ± 0.14 ^a	3.03 ± 0.04 ^b
RV weight (mg)	197.0 ± 0.01	303.0 ± 0.02 ^a	219.5 ± 0.01 ^b
RV weight to body weight ratio	0.48 ± 0.02	0.88 ± 0.07 ^a	0.62 ± 0.03 ^{a,b}

Data is represented as mean ± standard error of mean.

^aSignificantly different from control animals.

^bsignificantly different from the MCT only group ($P < 0.05$). $n = 6$ animals/group.